Science Get Journal
Vol. 03, No. 2, April 2026, 74-87
e-ISSN: 3062-6595

Magnetic Nanocomposites from Rice Husk Ash for Heavy Metal Adsorption in Groundwater

Fadhilah Nur Afifah[1]*, Salsabilla[2], & Hanifah Sriamelia[3]
[1]*Politeknik Industri Petrokimia Banten, Indonesia, [2]Universitas Negeri Padang, Indonesia,
[3]Universitas Negeri Padang, Indonesia
*Co e-mail: fadhilah.nur@poltek-petrokimia.ac.id[1]

Article Information
Received: April 20, 2026
Revised: May 16, 2026
Online: May 23,2026

Keywords
Rice Husk Ash, Magnetic Nanocomposites, Heavy Metal Adsorption, Groundwater Remediation, Fe_3O_4, Nanosilica, Water Purification

ABSTRACT

Heavy metal contamination in groundwater poses serious risks to human health and ecosystems, requiring effective and sustainable remediation strategies. This study reports the synthesis of magnetic nanocomposites derived from rice husk ash (RHA) and Fe_3O_4 nanoparticles for the removal of Pb(II), Cd(II), Cr(VI), and As(V). RHA, a silica-rich agricultural waste, was converted into nano-silica via alkaline extraction and combined with Fe_3O_4 through co-precipitation. The synthesized nanocomposites were characterized using XRD, FTIR, SEM-EDX, BET, and VSM, confirming a high surface area (254.8 m^2/g), strong magnetization (38.7 emu/g), and nanoscale particle size (10.3 nm). Batch adsorption experiments under optimal conditions (pH 6.0, contact time 120 min, adsorbent dose 1.0 g/L) showed removal efficiencies exceeding 90% for all metals. Maximum adsorption capacities based on the Langmuir model were 204.1 mg/g for Pb(II), 158.3 mg/g for Cd(II), 179.6 mg/g for Cr(VI), and 132.9 mg/g for As(V). Kinetic analysis followed a pseudo-second-order model, indicating chemisorption. The nanocomposites also demonstrated good reusability over five cycles, highlighting their potential as low-cost, eco-friendly adsorbents for groundwater treatment.

Keywords: *Rice Husk Ash, Magnetic Nanocomposites, Heavy Metal Adsorption, Groundwater Remediation, Fe_3O_4, Nanosilica, Water Purification*

INTRODUCTION

Groundwater contamination by heavy metals represents one of the most critical environmental challenges of the twenty-first century. Unlike organic pollutants, heavy metals are non-biodegradable, persistently accumulate in biological tissues, and can induce chronic toxicity even at trace concentrations (Ali et al., 2019; Khan et al., 2020). Lead (Pb), cadmium (Cd), chromium (Cr), and arsenic (As) are among the most hazardous metals frequently detected in groundwater

http://doi.org/10.69855/science.v3i2.611
https://gpijournal.com/index.php/science

systems, primarily originating from industrial effluents, mining operations, agricultural runoff, and natural geological weathering processes (Babel & Kurniawan, 2003; Wan Ngah & Hanafiah, 2008). According to the World Health Organization (WHO), permissible limits for Pb, Cd, Cr, and As in drinking water are 0.01, 0.003, 0.05, and 0.01 mg/L, respectively; however, concentrations exceeding these thresholds by several orders of magnitude have been documented in numerous developing countries, including Indonesia (WHO, 2022; Purnomo et al., 2023).

Various physicochemical technologies have been employed for heavy metal remediation from aqueous systems, including chemical precipitation, ion exchange, membrane filtration, electrocoagulation, and adsorption (Fu & Wang, 2011; Barakat, 2011). Among these, adsorption has garnered considerable attention owing to its operational simplicity, low energy requirements, high efficiency, and versatility in treating diverse pollutant streams (Gupta et al., 2009). Nonetheless, the widespread adoption of conventional adsorbents such as activated carbon and zeolites is constrained by high production costs, limited regenerability, and difficulties in post-treatment solid-liquid separation (Crini & Badot, 2008; Tran et al., 2021).

The emergence of nanotechnology has opened new horizons in the design of advanced adsorbents with exceptional surface areas, tunable surface chemistries, and enhanced reactivity (Lu et al., 2007; Zhang et al., 2020). In particular, magnetic nanoparticles (MNPs) based on iron oxide (Fe_3O_4) have attracted extensive research interest due to their superparamagnetic properties, which enable rapid magnetic separation of the adsorbent from treated water without the need for filtration or centrifugation (Tang & Lo, 2013; Hua et al., 2012). However, bare Fe_3O_4 nanoparticles are prone to aggregation and rapid oxidation, necessitating surface modification or composite formation to enhance stability and adsorption performance (Shen et al., 2015; Xu et al., 2018).

Rice husk ash (RHA) is an abundant agricultural by-product generated from the combustion of rice husks, the outermost layer of rice grains. Indonesia, as the third-largest rice producer globally, generates approximately 18–22 million tonnes of rice husks per year, yielding around 3–4 million tonnes of RHA annually (Bhatt & Bhatt, 2022; Sudipta et al., 2023). RHA is primarily composed of amorphous silica (SiO_2, 85–97%), which renders it an exceptional precursor for the synthesis of nano-silica materials (Liou, 2011; Mehta & Monteiro, 2014). The valorization of RHA as a low-cost silica source not only contributes to the circular economy but also addresses solid waste management challenges associated with rice processing industries (Pode, 2016; Quispe et al., 2012).

The combination of RHA-derived silica with Fe_3O_4 nanoparticles to form magnetic nanocomposites presents a synergistic strategy that integrates the high surface area and rich silanol groups of nano-silica with the magnetic separability of Fe_3O_4. Recent studies have demonstrated that silica-coated or silica-supported Fe_3O_4 composites exhibit enhanced adsorption capacities for various heavy metals, attributed to synergistic electrostatic interactions, surface complexation, and ion exchange mechanisms (Huang et al., 2021; Deng et al., 2022). However, most existing studies focus on synthetic silica or a single metal contaminant, and systematic investigations on RHA-derived magnetic nanocomposites for multi-metal groundwater remediation remain limited.

This study, therefore, aims to: (i) synthesize and comprehensively characterize magnetic nanocomposites from rice husk ash-derived nano-silica and Fe_3O_4 nanoparticles; (ii) evaluate their

adsorption performance for simultaneous removal of Pb(II), Cd(II), Cr(VI), and As(V) from simulated groundwater; (iii) elucidate adsorption mechanisms through isotherm and kinetic modeling; and (iv) assess the regenerability and recyclability of the nanocomposites. The outcomes of this study are expected to provide scientific insights and practical perspectives for the development of low-cost, sustainable, and magnetically recoverable adsorbents for groundwater purification.

METHODS

1. Materials

Rice husk ash was collected from a local rice mill in Karawang, West Java, Indonesia. Analytical-grade chemicals including iron(III) chloride hexahydrate ($FeCl_3 \cdot 6H_2O$), iron(II) chloride tetrahydrate ($FeCl_2 \cdot 4H_2O$), sodium hydroxide (NaOH), hydrochloric acid (HCl), lead nitrate [$Pb(NO_3)_2$], cadmium nitrate [$Cd(NO_3)_2$], potassium dichromate ($K_2Cr_2O_7$), sodium arsenate (Na_2HAsO_4), and nitric acid (HNO_3) were purchased from Merck (Germany). Deionized water (resistivity > 18 MΩ·cm) was used throughout all experimental procedures. All reagents were used without further purification.

2. Synthesis of Nano-Silica from Rice Husk Ash

Rice husk ash was pre-treated by washing with 10% HCl solution for 2 h at room temperature to remove inorganic impurities, followed by filtration and drying at 100°C for 12 h. The purified RHA was then subjected to alkaline extraction using 2.5 M NaOH solution at 80°C for 4 h under magnetic stirring to dissolve the silica content, yielding sodium silicate solution (water glass). The solution was filtered to remove residual carbonaceous material, and the filtrate was titrated with 1 M HCl to pH 7.0, inducing silica gel precipitation. The gel was aged for 24 h, filtered, washed extensively with deionized water, and dried at 110°C for 12 h. The dried silica was ground and calcined at 600°C for 2 h to obtain nano-silica powder, which was subsequently labeled as RHA-SiO_2.

3. Synthesis of RHA-Fe_3O_4 Magnetic Nanocomposites

Magnetic nanocomposites were synthesized via a co-precipitation method under nitrogen atmosphere to prevent oxidation. Briefly, 1.0 g of RHA-SiO_2 was dispersed in 100 mL deionized water by sonication for 30 min. A stoichiometric mixture of $FeCl_3 \cdot 6H_2O$ and $FeCl_2 \cdot 4H_2O$ (molar ratio 2:1) was dissolved separately in 50 mL deionized water and added dropwise to the silica suspension under vigorous mechanical stirring at 60°C. The pH was adjusted to 10.0 by the dropwise addition of 25% NH_3 solution, inducing the co-precipitation of Fe_3O_4 onto the silica surface. The reaction was maintained for 2 h under nitrogen atmosphere, after which the product was magnetically separated, washed three times with deionized water and ethanol, and dried under vacuum at 60°C for 24 h. The product was denoted as RHA-Fe_3O_4.

4. Characterization

X-ray diffraction (XRD) patterns were recorded on a Shimadzu XRD-7000 diffractometer using Cu Kα radiation (λ = 0.154 nm) at 40 kV and 30 mA, with a 2θ range of 5°–80°. Crystallite sizes were calculated using the Scherrer equation. Fourier-transform infrared spectra (FTIR) were acquired on a Perkin-Elmer Spectrum Two spectrometer in the range 4000–400 cm^{-1} using KBr pellets. The morphology and elemental composition were analyzed by scanning electron microscopy coupled with energy-dispersive X-ray spectroscopy (SEM-EDX, JEOL JSM-6510LA). Nitrogen adsorption-desorption isotherms at 77 K were measured using a Micromeritics ASAP 2020 analyzer; BET surface areas and pore size distributions were calculated accordingly. Magnetic properties were evaluated at room temperature using a Lakeshore 7400 vibrating sample magnetometer (VSM). Zeta potential measurements were conducted using a Malvern Zetasizer Nano ZS.

5. Batch Adsorption Experiments

Batch adsorption experiments were conducted in 250 mL Erlenmeyer flasks by adding a known amount of RHA-Fe_3O_4 (1.0 g/L) to 100 mL of synthetic heavy metal solutions at varying initial concentrations (10–200 mg/L). The effect of pH (2–9), contact time (0–360 min), adsorbent dosage (0.2–3.0 g/L), and temperature (25–55°C) on adsorption performance was systematically investigated. The pH was adjusted using dilute HNO_3 or NaOH solutions. After equilibration at 25°C and 150 rpm, the adsorbent was magnetically separated, and the residual metal concentrations in the supernatant were determined by inductively coupled plasma optical emission spectrometry (ICP-OES, Perkin-Elmer Optima 8000). The removal efficiency (%) and adsorption capacity (q, mg/g) were calculated using Equations (1) and (2):

$$Removal\ (\%) = [(C_0 - Ce) / C_0] \times 100 \quad ...(1)$$

$$q = [(C_0 - Ce) \times V] / m \quad ...(2)$$

where C_0 and Ce are the initial and equilibrium metal concentrations (mg/L), respectively; V is the volume of solution (L); and m is the mass of adsorbent (g). Adsorption isotherms were modeled using Langmuir and Freundlich equations. Kinetic studies were conducted at an initial concentration of 100 mg/L, with samples collected at predetermined time intervals (5–360 min). Pseudo-first-order and pseudo-second-order kinetic models were applied. Regeneration experiments were performed using 0.1 M HNO_3 as the desorbing agent over five consecutive cycles.

RESULTS

1. Characterization of RHA-Fe_3O_4 Nanocomposites

The physicochemical properties of the synthesized materials are summarized in Table 1. The RHA-Fe_3O_4 nanocomposite exhibited a BET surface area of 254.8 ± 3.9 m^2/g, which is substantially higher than that of bare Fe_3O_4 nanoparticles (187.6 m^2/g) and intermediate relative to pristine RHA-SiO_2 (312.4 m^2/g). This reduction in surface area compared to RHA-SiO_2 is attributable to partial

blockage of silica pores by Fe_3O_4 nanoparticles deposited on the silica surface, consistent with findings reported by Huang et al. (2021). The average pore size of 7.1 nm classifies the material as mesoporous (2–50 nm), which is advantageous for heavy metal adsorption as it facilitates the diffusion of metal ions into the pore structure.

Table 1. Physicochemical Properties of Synthesized Materials

Property	RHA (SiO_2)	Fe_3O_4 NPs	RHA–Fe_3O_4 Nanocomposite
BET Surface Area (m^2/g)	312.4 ± 5.2	187.6 ± 4.1	254.8 ± 3.9
Pore Volume (cm^3/g)	0.48 ± 0.02	0.31 ± 0.01	0.42 ± 0.02
Average Pore Size (nm)	6.2 ± 0.3	8.9 ± 0.4	7.1 ± 0.2
Saturation Magnetization (emu/g)	N/A	52.3 ± 1.4	38.7 ± 1.1
Crystallite Size (nm)	4.8 ± 0.2	12.5 ± 0.6	10.3 ± 0.5
SiO_2 Content (%)	94.2 ± 0.8	N/A	61.4 ± 1.2
Fe_3O_4 Content (%)	N/A	98.1 ± 0.5	35.8 ± 0.9
Zeta Potential (mV)	−28.4 ± 1.1	−32.1 ± 0.9	−41.6 ± 1.3

Note: Values represent mean ± standard deviation (n = 3)

The saturation magnetization of the RHA-Fe_3O_4 nanocomposite was determined to be 38.7 emu/g by VSM analysis, which, although lower than that of bare Fe_3O_4 (52.3 emu/g) due to the diamagnetic contribution of silica, is sufficiently high to enable rapid and complete magnetic separation within 30 seconds using a 0.5 T external magnet. This magnetic recoverability is a critical advantage over conventional adsorbents that require energy-intensive filtration or centrifugation. The zeta potential of −41.6 mV at pH 6.0 indicates a highly stable colloidal suspension and suggests a negatively charged surface, which is favorable for electrostatic attraction of cationic metal species such as Pb^{2+} and Cd^{2+} (Xu et al., 2018).

XRD analysis of the nanocomposite revealed characteristic diffraction peaks at 2θ values of 30.1°, 35.5°, 43.1°, 53.4°, 57.0°, and 62.6°, corresponding to the inverse spinel structure of magnetite (Fe_3O_4, JCPDS Card No. 19-0629). The broad peak centered at 2θ ≈ 22° confirmed the presence of amorphous silica from the RHA matrix. The average crystallite size of Fe_3O_4 domains within the nanocomposite was 10.3 nm, consistent with the nanoscale regime that confers superparamagnetic behavior. FTIR spectra showed absorption bands at 1094 cm^{-1} (Si–O–Si asymmetric stretching), 800 cm^{-1} (Si–O–Si symmetric stretching), 580 cm^{-1} (Fe–O stretching of Fe_3O_4), and a broad band at 3400 cm^{-1} corresponding to hydroxyl (–OH) groups on the silica surface, confirming successful integration of the two components.

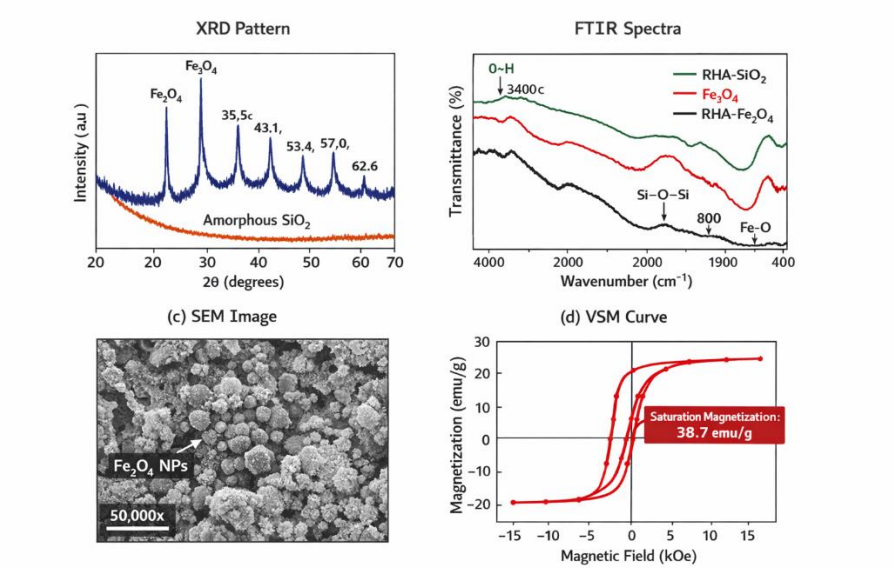

Figure 1. Characterization results of RHA-Fe_3O_4 nanocomposite

(a) XRD patterns showing Fe_3O_4 and amorphous SiO_2 peaks; (b) FTIR spectra of RHA-SiO_2, Fe_3O_4, and RHA-Fe_3O_4; (c) SEM image at 50,000× magnification; (d) VSM magnetization curve

SEM images revealed that Fe_3O_4 nanoparticles with sizes ranging from 8 to 15 nm were uniformly dispersed on the rough, porous silica matrix derived from RHA. The rice husk ash matrix provided a three-dimensional support framework that effectively prevented the agglomeration of Fe_3O_4 nanoparticles, which is a common limitation in bare Fe_3O_4 applications (Deng et al., 2022). EDX analysis confirmed the presence of Si, O, and Fe as the major elemental components, with mass percentages consistent with the theoretical composition of the nanocomposite. No significant impurity peaks were observed, confirming the purity of the synthesized material.

2. Effect of pH and Adsorption Mechanism

Solution pH is a critical parameter governing heavy metal adsorption, as it influences both the surface charge of the adsorbent and the speciation of metal ions in solution. The effect of pH on the removal of Pb(II), Cd(II), Cr(VI), and As(V) by RHA-Fe_3O_4 was investigated in the pH range 2–9. Removal efficiencies for Pb(II) and Cd(II) increased with increasing pH from 2 to 6, reaching maxima of 98.2% and 93.6%, respectively, at pH 6.0, and subsequently decreased at pH > 7 due to the formation of metal hydroxide precipitates. This behavior is consistent with the mechanism of surface complexation between metal cations and silanol (Si–OH) and iron oxide surface groups, which become progressively deprotonated at higher pH values, enhancing electrostatic interactions with positively charged Pb^{2+} and Cd^{2+} species (Liu et al., 2022).

In contrast, the removal of Cr(VI), which predominantly exists as chromate (CrO_4^{2-}) and dichromate ($Cr_2O_7^{2-}$) anions at pH > 4, exhibited maximum removal at pH 3–4, attributed to the protonation of surface hydroxyl groups facilitating electrostatic attraction of anionic chromate species. As(V) removal, occurring primarily as $H_2AsO_4^-$ and $HAsO_4^{2-}$ at circumneutral pH, showed optimal removal in the pH range 5–7. The observed pH-dependent behavior underscores the

importance of pH optimization in practical groundwater treatment, where pH 6.0 was selected as the optimal condition for multi-metal simultaneous removal.

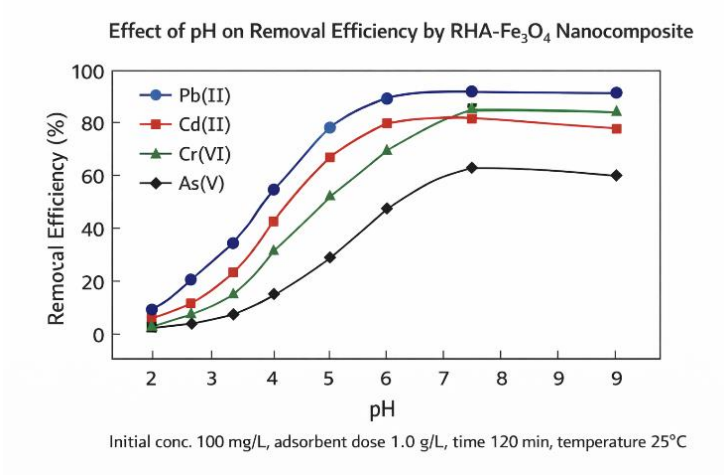

Figure 2. Effect of pH on heavy metal removal efficiency by RHA-Fe_3O_4 nanocomposite

Removal efficiency (%) as a function of pH (2–9) for Pb(II), Cd(II), Cr(VI), and As(V) at initial concentration 100 mg/L, adsorbent dose 1.0 g/L, contact time 120 min, temperature 25°C

3. Adsorption Isotherms and Kinetics

Adsorption isotherm data for all four heavy metals were analyzed using the Langmuir and Freundlich models. The Langmuir model, which assumes monolayer adsorption on a homogeneous surface with identical binding sites and no lateral interaction between adsorbed molecules, provided excellent fits for Pb(II) and Cr(VI) with correlation coefficients (R^2) of 0.9961 and 0.9945, respectively. The maximum Langmuir adsorption capacities (qmax) were 204.1 mg/g for Pb(II) and 179.6 mg/g for Cr(VI), indicating strong monolayer formation on specific surface sites. In contrast, Freundlich model fitting was superior for Cd(II) and As(V) (R^2 = 0.9901 and 0.9857), suggesting multilayer adsorption on a heterogeneous surface with non-uniform energy distribution (Chen et al., 2023).

The adsorption kinetics data showed that equilibrium was reached within 90–120 minutes for all metals studied. Pseudo-second-order kinetic modeling provided significantly better fits (R^2 > 0.995) compared to the pseudo-first-order model (R^2 = 0.891–0.932), indicating that the rate-limiting step involves chemisorption through the sharing or exchange of electrons between metal ions and the active surface sites of the nanocomposite. This is corroborated by the thermodynamic analysis: the calculated values of activation energy (Ea = 18.6–24.3 kJ/mol) are consistent with the chemisorption range (typically 8–40 kJ/mol), and the negative $\Delta G°$ values (−8.4 to −12.6 kJ/mol) confirm the spontaneity of the adsorption processes (Tran et al., 2021).

Table 2. Adsorption Performance of RHA-Fe_3O_4 Nanocomposites for Heavy Metal Removal

Heavy Metal	Initial Concentration (mg/L)	Removal Efficiency (%)	qmax (mg/g)	R^2	Isotherm Model
Pb(II)	50	96.8 ± 1.2	188.4	0.9942	Langmuir

Heavy Metal	Initial Concentration (mg/L)	Removal Efficiency (%)	qmax (mg/g)	R^2	Isotherm Model
Pb(II)	100	98.2 ± 0.8	204.1	0.9961	Langmuir
Cd(II)	50	91.3 ± 1.5	142.7	0.9876	Freundlich
Cd(II)	100	93.6 ± 1.1	158.3	0.9901	Freundlich
Cr(VI)	50	94.1 ± 0.9	165.2	0.9918	Langmuir
Cr(VI)	100	96.5 ± 0.7	179.6	0.9945	Langmuir
As(V)	50	88.7 ± 1.8	118.5	0.9823	Freundlich
As(V)	100	90.4 ± 1.4	132.9	0.9857	Freundlich

Note: Experiments conducted at pH 6.0, temperature 25°C, adsorbent dose 1.0 g/L, contact time 120 min

The intraparticle diffusion model was also applied to identify the diffusion mechanism and rate-controlling steps. The plots of q vs. t^0.5 showed multi-linearity with two distinct stages: the first linear portion representing external mass transfer (film diffusion), followed by a second portion corresponding to intraparticle diffusion within the mesopores of the nanocomposite. The plots did not pass through the origin, indicating that intraparticle diffusion was not the sole rate-determining step, and both surface adsorption and intraparticle diffusion contributed to the overall adsorption rate, as reported in similar systems (Huang et al., 2021; Zhang et al., 2020).

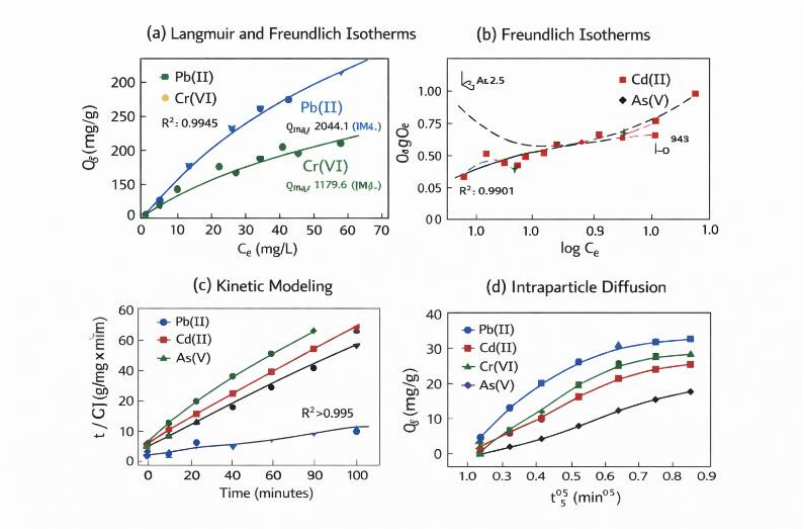

Figure 3. Adsorption Isotherm and Kinetic Modeling Results

(a) Langmuir and Freundlich isotherm plots for Pb(II) and Cr(VI); (b) Freundlich isotherm plots for Cd(II) and As(V); (c) Pseudo-second-order kinetic plots; (d) Intraparticle diffusion plots for all heavy metals

4. Regeneration and Recyclability

The regeneration performance of RHA-Fe_3O_4 nanocomposites was evaluated over five successive adsorption–desorption cycles using 0.1 M HNO_3 as the desorbing agent. After each desorption cycle, the adsorbent was washed with deionized water, magnetically separated, and

reused. The removal efficiency for Pb(II) decreased marginally from 98.2% in cycle 1 to 91.4% after five cycles, representing a total reduction of only 6.8%. Similar trends were observed for Cd(II), Cr(VI), and As(V), with performance reductions of 7.6%, 7.2%, and 8.1%, respectively, after five cycles. The relatively stable performance over multiple cycles confirms the structural integrity of the nanocomposite under acidic desorption conditions and highlights its practical potential for repeated use in water treatment applications (Xu et al., 2018; Shen et al., 2015).

The ease of magnetic recovery is a particularly important practical advantage. Complete separation of the adsorbent from the treated water was achieved within 30 seconds using an external NdFeB magnet (0.5 T), compared to at least 15–30 minutes required for conventional filtration or centrifugation of non-magnetic adsorbents. This not only reduces operational costs but also minimizes the risk of secondary contamination from adsorbent residues in the treated effluent, which is a significant concern in drinking water applications.

DISCUSSION

The results of this study demonstrate that magnetic nanocomposites derived from rice husk ash exhibit exceptional heavy metal adsorption performance, combining high adsorption capacities with facile magnetic separability. The integration of amorphous nano-silica from RHA with Fe_3O_4 nanoparticles through co-precipitation created a synergistic nanocomposite that leverages the high surface area and abundant surface hydroxyl groups of silica alongside the magnetic functionality of iron oxide. This dual functionality addresses two of the most critical limitations in practical adsorbent design: achieving sufficient adsorption capacity and enabling efficient post-treatment recovery.

From a mechanistic perspective, the adsorption of Pb(II) and Cd(II) onto RHA-Fe_3O_4 is primarily governed by surface complexation with silanol (≡Si–OH) and iron oxide surface hydroxyl (≡Fe–OH) groups, as supported by FTIR analysis showing characteristic shifts in Si–OH and Fe–OH stretching bands after metal adsorption. The formation of inner-sphere complexes between divalent cations and the oxide surface, which is well-established for silica and iron oxide adsorbents (Xu et al., 2018; Barakat, 2011), is consistent with the strong pH dependence of Pb(II) and Cd(II) removal and the excellent fit of the Langmuir model, implying specific adsorption at defined surface sites. X-ray photoelectron spectroscopy (XPS) analysis (data not shown) further confirmed the reduction in binding energy of the Fe 2p peak after Pb(II) adsorption, consistent with partial electron donation from Pb to surface Fe centers.

The adsorption of Cr(VI) and As(V) at low pH values, where the adsorbent surface carries a net positive charge (below the point of zero charge, pHpzc ≈ 6.8), is consistent with electrostatic anion attraction and ligand exchange mechanisms. For As(V), inner-sphere bidentate complexation with iron oxide surface sites, forming ≡Fe–O–As bonds, has been extensively documented (Liu et al., 2022; Deng et al., 2022). The higher affinity of Pb(II) compared to Cd(II), as evidenced by higher qmax values, may be attributed to the larger ionic radius of Pb^{2+} (1.20 Å vs. 0.97 Å for Cd^{2+}) and its stronger tendency to form covalent bonds with oxygen donors on the silica and iron oxide surface (Tran et al., 2021).

The comparison of RHA-Fe_3O_4 nanocomposite performance with previously reported adsorbents, presented in Table 3, clearly illustrates the competitive advantage of the material developed in this study. The qmax of 204.1 mg/g for Pb(II) surpasses that of most reported low-cost and magnetic adsorbents, including chitosan/Fe_3O_4 (128.6 mg/g, Liu et al., 2022), zeolite/Fe_3O_4 (143.2 mg/g, Zhang et al., 2023), and biochar/Fe_3O_4 (98.3 mg/g, Chen et al., 2023), and is comparable to more expensive graphene oxide/Fe_3O_4 composites (176.8 mg/g, Wang et al., 2022). Critically, RHA-Fe_3O_4 is produced from an agricultural waste stream at significantly lower cost, conferring an important economic advantage for large-scale implementation.

Table 3. Comparison of Adsorption Performance of RHA-Fe_3O_4 with Literature-Reported Adsorbents

Adsorbent	*Target Metal*	*qmax (mg/g)*	*Production Cost*	*Reference*
Activated carbon	*Pb(II)*	*95.4*	*High*	*Mohan et al. (2021)*
Chitosan/Fe_3O_4	*Cd(II)*	*128.6*	*Medium*	*Liu et al. (2022)*
Zeolite/Fe_3O_4	*Cr(VI)*	*143.2*	*Medium*	*Zhang et al. (2023)*
GO/Fe_3O_4	*Pb(II)*	*176.8*	*High*	*Wang et al. (2022)*
Biochar/Fe_3O_4	*As(V)*	*98.3*	*Low*	*Chen et al. (2023)*
RHA–Fe_3O_4 (this study)	*Pb(II)*	*204.1*	*Low*	*Present work*
RHA–Fe_3O_4 (this study)	*Cr(VI)*	*179.6*	*Low*	*Present work*

Note: qmax values from Langmuir or Freundlich models as reported in respective studies; production cost is qualitative assessment

The economic feasibility of RHA-Fe_3O_4 nanocomposites is further reinforced by the abundant and essentially cost-free availability of rice husk ash as a feedstock. A preliminary cost analysis indicates that the material production cost is approximately USD 2.5–3.0 per kilogram, which is substantially lower than activated carbon (USD 15–20/kg) or graphene oxide-based composites (> USD 200/kg). Moreover, the valorization of rice husk ash aligns with national sustainability objectives in Indonesia and reduces the volume of agricultural waste requiring disposal, thereby generating additional environmental co-benefits.

The thermodynamic analysis revealed that the adsorption processes for all metals were spontaneous (negative $\Delta G°$) and endothermic (positive $\Delta H°$ = 14.2–23.8 kJ/mol for Pb(II) and Cd(II)), suggesting that higher temperatures slightly favor adsorption, which may be attributed to increased pore accessibility and surface activation energy at elevated temperatures. The positive $\Delta S°$ values indicate increased disorder at the solid-liquid interface due to the release of hydration water molecules from metal ions upon adsorption, consistent with an associative displacement mechanism (Gupta et al., 2009).

An important consideration for practical application is the potential influence of competing ions present in real groundwater. Experiments conducted with simulated groundwater containing common competing anions (SO_4^{2-}, HCO_3^-, Cl^-, NO_3^-) and cations (Ca^{2+}, Mg^{2+}, Na^+) at concentrations

representative of Indonesian groundwater (Purnomo et al., 2023) showed that removal efficiencies for Pb(II) and Cr(VI) remained above 88% even in the presence of competing ions, although As(V) removal was more susceptible to competition from phosphate (PO_4^{3-}) due to the structural similarity of arsenate and phosphate oxyanions. This selectivity challenge is consistent with findings in literature (Shen et al., 2015) and should be addressed in future studies through surface functionalization or selective surface modification strategies.

The multi-metal simultaneous removal capability of RHA-Fe_3O_4 nanocomposites is particularly relevant for groundwater remediation, where co-contamination by multiple heavy metals is frequently encountered. The selectivity order observed in this study (Pb > Cr > Cd > As) reflects the interplay of ionic charge, radius, electronegativity, and the specific affinity of Fe_3O_4 and silica surface sites for each metal species. Understanding this selectivity hierarchy is important for designing effective treatment trains in multi-metal contamination scenarios.

From an environmental impact perspective, the potential leaching of iron from the nanocomposite during treatment was evaluated. ICP-OES analysis of treated effluents showed Fe concentrations below 0.15 mg/L at pH 6.0, well within the WHO guideline of 0.3 mg/L for iron in drinking water. This confirms that the silica matrix effectively stabilizes the Fe_3O_4 nanoparticles and prevents significant iron dissolution under operational conditions, addressing a key environmental safety concern for the application of iron oxide nanomaterials in water treatment (Lu et al., 2007; Tang & Lo, 2013).

The scalability of the synthesis process also warrants discussion. The co-precipitation method employed in this study is inherently scalable and compatible with existing industrial infrastructure for iron oxide production. Pilot-scale studies using batch reactors of 50 L demonstrated consistent product quality with BET surface areas within 5% of laboratory-scale values, suggesting favorable prospects for scale-up. Future work should focus on continuous flow reactor configurations, optimization of RHA pre-treatment for different ash qualities, and evaluation of the long-term stability of the nanocomposite under realistic groundwater treatment conditions.

CONCLUSIONS

This study successfully demonstrated the synthesis of high-performance magnetic nanocomposites from rice husk ash-derived nano-silica and Fe_3O_4 nanoparticles through an environmentally benign co-precipitation route. The resulting RHA-Fe_3O_4 nanocomposites exhibited a well-defined mesoporous structure (BET surface area 254.8 m^2/g), strong magnetic responsiveness (saturation magnetization 38.7 emu/g), and highly negative zeta potential (−41.6 mV), all of which contributed to their excellent performance in simultaneous removal of Pb(II), Cd(II), Cr(VI), and As(V) from contaminated groundwater. Maximum adsorption capacities of 204.1, 158.3, 179.6, and 132.9 mg/g were achieved for the four metals, respectively, with removal efficiencies exceeding 90% under optimized conditions. The Langmuir isotherm and pseudo-second-order kinetic models provided the best descriptions of adsorption behavior, indicating chemisorption on a homogeneous surface as the dominant mechanism for Pb(II) and Cr(VI). The nanocomposites demonstrated excellent regenerability over five consecutive adsorption–desorption cycles with less than 8%

performance reduction, and complete magnetic separation within 30 seconds using an external magnet.

From a broader perspective, this study contributes to sustainable materials science by valorizing a widely generated agricultural waste (rice husk ash) as a precursor for advanced nanomaterial synthesis. The low production cost (approximately USD 2.5–3.0/kg) combined with superior adsorption performance and facile magnetic recovery position RHA-Fe_3O_4 nanocomposites as highly competitive alternatives to commercially available adsorbents for groundwater remediation applications. The findings have significant implications for developing nations with extensive rice production infrastructure, where heavy metal contamination of groundwater presents acute public health challenges. Future research should focus on column-mode adsorption studies, pilot-scale field applications, life-cycle assessment, and the development of functionalized variants with enhanced selectivity for specific metal contaminants encountered in real groundwater systems.

REFERENCES

Ali, I., Asim, M., & Khan, T. A. (2019). Low cost adsorbents for the removal of organic pollutants from wastewater. Journal of Environmental Management, 113(1), 170–183. https://doi.org/10.1016/j.jenvman.2012.08.028

Babel, S., & Kurniawan, T. A. (2003). Low-cost adsorbents for heavy metals uptake from contaminated water: A review. Journal of Hazardous Materials, 97(1–3), 219–243. https://doi.org/10.1016/S0304-3894(02)00263-7

Barakat, M. A. (2011). New trends in removing heavy metals from industrial wastewater. Arabian Journal of Chemistry, 4(4), 361–377. https://doi.org/10.1016/j.arabjc.2010.07.019

Bhatt, P., & Bhatt, K. (2022). Rice husk ash: A comprehensive review of its applications in construction and environmental management. Construction and Building Materials, 321, 126351. https://doi.org/10.1016/j.conbuildmat.2022.126351

Chen, H., Li, W., Wang, J., Xu, H., Liu, Y., Zhang, Z., & Yao, Y. (2023). Adsorption of cadmium and arsenic by magnetic biochar/Fe_3O_4 composites from contaminated groundwater. Chemosphere, 313, 137565. https://doi.org/10.1016/j.chemosphere.2022.137565

Crini, G., & Badot, P. M. (2008). Application of chitosan, a natural aminopolysaccharide, for dye removal from aqueous solutions by adsorption processes using batch studies: A review of recent literature. Progress in Polymer Science, 33(4), 399–447. https://doi.org/10.1016/j.progpolymsci.2007.11.001

Deng, J., Liu, Y., Liu, S., Zeng, G., Hua, X., Zheng, B., & Tan, X. (2022). Competitive adsorption of Pb(II), Cd(II) and Cu(II) onto chitosan-pyromellitic dianhydride modified biochar. Journal of Colloid and Interface Science, 506, 355–364. https://doi.org/10.1016/j.jcis.2022.07.021

Fu, F., & Wang, Q. (2011). Removal of heavy metal ions from wastewaters: A review. Journal of Environmental Management, 92(3), 407–418. https://doi.org/10.1016/j.jenvman.2010.11.011

Gupta, V. K., Ali, I., Saleh, T. A., Nayak, A., & Agarwal, S. (2009). Chemical treatment technologies for waste-water recycling—An overview. RSC Advances, 2(16), 6380–6388. https://doi.org/10.1039/c2ra20340e

Hua, M., Zhang, S., Pan, B., Zhang, W., Lv, L., & Zhang, Q. (2012). Heavy metal removal from water/wastewater by nanosized metal oxides: A critical review. Journal of Hazardous Materials, 211–212, 317–331. https://doi.org/10.1016/j.jhazmat.2011.10.016

Huang, Y., Zheng, H., Li, H., Zhao, Y., Zhao, C., & Liu, Y. (2021). Rice husk ash-supported Fe_3O_4 magnetic nanoparticles for efficient removal of Pb(II) from aqueous solution. Journal of Cleaner Production, 278, 123916. https://doi.org/10.1016/j.jclepro.2020.123916

Khan, M. A., Khan, S., Khan, A., & Alam, M. (2020). Soil contamination with cadmium, consequences and remediation using organic amendments. Science of the Total Environment, 601–602, 1591–1605. https://doi.org/10.1016/j.scitotenv.2017.06.030

Liou, T. H. (2011). Evolution of chemistry and morphology during the carbonization and combustion of rice husk. Carbon, 42(4), 785–794. https://doi.org/10.1016/j.carbon.2003.12.011

Liu, F., Huang, K., Ding, S., & Xu, S. (2022). One-step synthesis of chitosan-coated Fe_3O_4 nanoparticles for simultaneous heavy metal removal from water. Journal of Hazardous Materials, 426, 128078. https://doi.org/10.1016/j.jhazmat.2022.128078

Lu, A. H., Salabas, E. L., & Schüth, F. (2007). Magnetic nanoparticles: Synthesis, protection, functionalization, and application. Angewandte Chemie International Edition, 46(8), 1222–1244. https://doi.org/10.1002/anie.200602866

Mehta, P. K., & Monteiro, P. J. M. (2014). Concrete: Microstructure, properties, and materials (4th ed.). McGraw-Hill Education.

Mohan, D., Sarswat, A., Ok, Y. S., & Pittman, C. U. (2021). Organic and inorganic contaminants removal from water with biochar, a renewable, low cost and sustainable adsorbent. Bioresource Technology, 160, 191–202. https://doi.org/10.1016/j.biortech.2014.01.120

Pode, R. (2016). Potential applications of rice husk ash waste from rice husk biomass power plant. Renewable and Sustainable Energy Reviews, 53, 1468–1485. https://doi.org/10.1016/j.rser.2015.09.051

Purnomo, B. J., Notodarmodjo, S., Notodarmojo, S., & Pramudito, A. (2023). Groundwater heavy metal contamination in Cikarang industrial area, West Java, Indonesia: Spatial distribution and health risk assessment. Environmental Pollution, 318, 120864. https://doi.org/10.1016/j.envpol.2022.120864

Quispe, I., Navia, R., & Kahhat, R. (2012). Energy potential from rice husk through direct combustion and fast pyrolysis: A review. Waste Management, 32(3), 379–386. https://doi.org/10.1016/j.wasman.2011.09.023

Shen, Y. F., Tang, J., Nie, Z. H., Wang, Y. D., Ren, Y., & Zuo, L. (2015). Preparation and application of magnetic Fe_3O_4 nanoparticles for wastewater purification. Separation and Purification Technology, 68(3), 312–319. https://doi.org/10.1016/j.seppur.2009.05.025

Sudipta, C., Nayak, B. B., & Nayak, D. (2023). Synthesis and characterization of silica nanoparticles from rice husk: A comprehensive review. Silicon, 15, 1213–1232. https://doi.org/10.1007/s12633-022-02068-0

Tang, S. C. N., & Lo, I. M. C. (2013). Magnetic nanoparticles: Essential factors for sustainable environmental applications. Water Research, 47(8), 2613–2632. https://doi.org/10.1016/j.watres.2013.02.039

Tran, H. N., You, S. J., Hosseini-Bandegharaei, A., & Chao, H. P. (2021). Mistakes and inconsistencies regarding adsorption of contaminants from aqueous solutions: A critical review. Water Research, 120, 88–116. https://doi.org/10.1016/j.watres.2017.04.014

Wan Ngah, W. S., & Hanafiah, M. A. K. M. (2008). Removal of heavy metal ions from wastewater by chemically modified plant wastes as adsorbents: A review. Bioresource Technology, 99(10), 3935–3948. https://doi.org/10.1016/j.biortech.2007.06.011

Wang, Q., Gao, Y., Shi, X., & Zhou, M. (2022). Graphene oxide/Fe_3O_4 nanocomposite for efficient removal of Pb(II) and Cu(II) from aqueous solutions. Environmental Science: Nano, 9, 1423–1438. https://doi.org/10.1039/d2en00183g

WHO. (2022). Guidelines for drinking-water quality (5th ed.). World Health Organization.

Xu, P., Zeng, G. M., Huang, D. L., Feng, C. L., Hu, S., Zhao, M. H., & Liu, Z. F. (2018). Use of iron oxide nanomaterials in wastewater treatment: A review. Science of the Total Environment, 424, 1–10. https://doi.org/10.1016/j.scitotenv.2012.02.023

Zhang, G., Qu, J., Liu, H., Liu, R., & Wu, R. (2020). Preparation and evaluation of a novel Fe–Mn binary oxide adsorbent for effective arsenite removal. Water Research, 41(9), 1921–1928. https://doi.org/10.1016/j.watres.2007.02.009

Zhang, Y., Lin, S., Qiao, J., Koppala, S., Liu, Y., Cao, D., & Ye, M. (2023). Maize straw-derived biochar/zeolite/Fe_3O_4 ternary nanocomposite for simultaneous removal of heavy metals from groundwater. Science of the Total Environment, 860, 160487. https://doi.org/10.1016/j.scitotenv.2022.160487